Wave reflections and resonance in a Mach 0.9 turbulent jet

Robin Prinja[1]†, Eduardo Martini[1], Peter Jordan[1], Aaron Towne[2] and André V. G. Cavalieri[3]

[1]Département Fluides, Thermique et Combustion, Institut Pprime, CNRS - Université de Poitiers, Poitiers, France

[2]Department of Mechanical Engineering, University of Michigan, Ann Arbor, MI 48109, USA

[3]Instituto Tecnológico de Aeronáutica, São José dos Campos/SP, Brazil

(Received xx; revised xx; accepted xx)

This work aims to provide a more complete understanding of the resonance mechanisms that occur in turbulent jets at high subsonic Mach number, as shown by Towne *et al.* (2017). Resonance was suggested by that study to exist between upstream- and downstream-travelling guided waves. Five possible resonance mechanisms were postulated, each involving different families of guided waves that reflect in the nozzle exit plane and a number of downstream turning points. But the study did not show which of these mechanisms are active in the flow. In this work, the waves underpinning resonance are identified via a biorthogonal projection of the Large Eddy Simulation data on eigenbases provided by locally parallel linear stability analysis. Two of the scenarios postulated by Towne *et al.* (2017) are thus confirmed to exist in the turbulent jet data. The reflection-coefficients in the nozzle exit and turning-point planes are, furthermore, identified.

1. Introduction

The mechanisms underpinning oscillator behaviour in fluid-mechanics problems can be classified as short- or long-ranged. Short-ranged mechanisms are typically associated with absolute instability (Huerre & Monkewitz 1985), observed for instance in wakes (Monkewitz & Sohn 1988) and hot jets (Huerre & Monkewitz 1990). Long-ranged mechanisms involve a pair of upstream- and downstream-travelling waves which interact at two end locations, where they are reflected into one another. If the wave amplitude increases over the cycle between two reflections, a long-range-resonant instability occurs. If the amplitude is unchanged, a neutrally stable mode is created, which, in turbulent flows, can be driven by the background turbulence. Such mechanisms have been observed in many different flows, such as when jets interact with edges (Powell 1953; Jordan *et al.* 2018), in cavity flows (Rockwell & Naudascher 1979; Rowley *et al.* 2002), impinging jets (Ho & Nosseir 1981; Tam & Ahuja 1990), shock-containing jets (Raman 1999; Edgington-Mitchell 2019), and high subsonic jets (Towne *et al.* 2017; Schmidt *et al.* 2017). The waves underpinning resonance can frequently be modelled using linear mean-flow analysis (Michalke 1970; Crighton & Gaster 1976; Jordan & Colonius 2013; Cavalieri *et al.* 2019).

In this study, we revisit the tones found in Mach 0.9 turbulent jets, postulated by Towne *et al.* (2017) to be driven by waves resonating between the nozzle exit and downstream turning points. The waves in question are guided waves of positive and negative generalised group velocities, denoted as k^+ and k^- respectively, as per Briggs (1964) and Bers (1983). The waves are neutrally stable at the resonance frequencies and

† Email address for correspondence: robin.prinja@univ-poitiers.fr

can be described using locally parallel linear stability analysis. Among the identified waves are the Kelvin-Helmhotz (hereafter K-H) instability wave (Michalke 1970) and neutrally stable guided waves (Towne *et al.* 2017; Martini *et al.* 2019). These guided waves consist of one downstream-travelling wave: the k^+ duct-like mode and two upstream-travelling waves: the k^- duct-like mode and k^- discrete free-stream mode.

At resonant frequencies, the k^+ and k^- waves propagate between the nozzle exit and turning point, exchanging energy through reflections at these end locations. The turning point is a downstream location characterized by the presence of a saddle point where a pair of k^+ and k^- waves share the same frequency and wavenumbers. Depending on the frequency, the k^+ wave can form a turning point with either of the k^- waves, resulting in two possible resonance mechanisms (Towne *et al.* 2017). The stability analysis (see section 3.1) reveals that, in the Strouhal range ($St = fD/U_j = \{0.23 - 0.47\}$, where f is the resonance frequency, U_j is the jet velocity, and D is the jet diameter), the k^+ duct-like mode forms a turning point with the k^- duct-like mode for lower frequencies, but with the k^- discrete free-stream mode for higher frequencies.

In the present work, we aim to conclusively establish if these frequency-dependent resonance mechanisms are active in the jet. We revisit the turbulent jet data with the goal of: (1) educing the waves present in the data; (2) establishing which of these underpin resonance; (3) computing the reflection-coefficients associated with energy exchange at the resonance end locations. This third objective is important for simplified resonance models, such as proposed by Jordan *et al.* (2018); Mancinelli *et al.* (2019, 2021).

The paper is organised as follows. Section 2 presents the Large Eddy Simulation (LES) database which is used. Local linear stability analysis is performed on the jet mean flow in section 3.1. The LES data is then decomposed using bi-orthogonal projections on the stability eigenbasis in section 3.2. It is shown how, at resonant conditions, the LES data can be represented by a rank-4 model. This is the basis for the calculation of reflection-coefficients at the resonance end locations. Section 4 presents the reflection-coefficient eduction methodology and section 5 presents the final results for a range of resonant frequencies.

2. LES database

We analyze LES data for a Mach $M = 0.9$ jet from Brès *et al.* (2018), where the guided waves have been observed in the potential-core region and associated discrete spectral tones have been detected in the near-nozzle region (Towne *et al.* 2017; Schmidt *et al.* 2017; Bogey 2021).

The data, described in Brès *et al.* (2018), covers a cylindrical grid with length $30D$ and radius $6D$. It contains 10000 timesteps over 2000 acoustic time units (tc/D, where c is sound speed), sampled every 0.2 acoustic time units. The cylindrical coordinate system has its origin centered on the jet axis in the nozzle plane.

LES time-series data is decomposed into Fourier modes,

$$\mathbf{q}_{LES}(x, r, \theta, t) = \sum_{\omega} \sum_{m} \hat{\mathbf{q}}_{LES}(x, r, m, \omega)\ e^{im\theta} e^{i\omega t}, \tag{2.1}$$

where x is the axial coordinate, r is the radial coordinate, m is the azimuthal wavenumber and ω is the angular frequency of fluctuation quantities. The time-series is split into 153 realisations, where each realisation contains 256 snapshots and an overlap of 75%. This leads to the frequency resolution of $\Delta St = \Delta f D/U_j = 0.0217$. Only the $m = 0$ mode is considered.

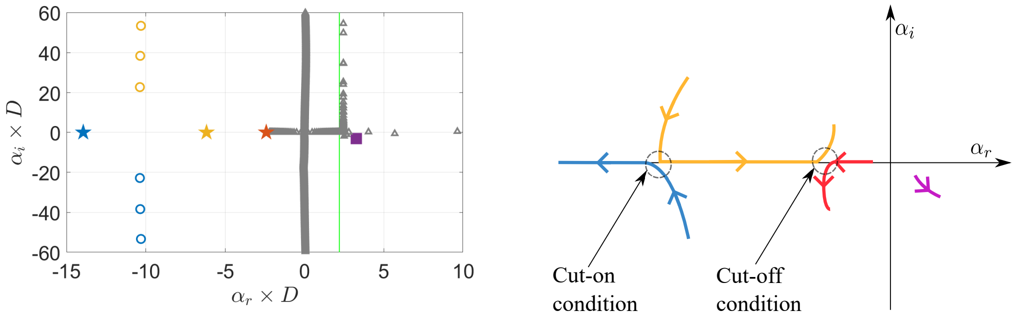

(a) Eigenspectrum for $St = 0.39$: ($\star$, blue) k_d^-; ($\star$, red) k_p^-; ($\star$, yellow) k_T^+; ($\blacksquare$, purple) k_{KH}^+; (—, light green) sonic line.

(b) Modes trajectories for St={0.23 → 0.47}: (—, blue) k_d^-; (—, red) k_p^-; (—, yellow) k_T^+; (—, purple) k_{KH}^+.

Figure 1: Linear stability analysis at $x/D = 0$, $m = 0$ for $M = 0.9$ jet.

3. Decomposing turbulent jet data into the resonating modes

To identify the waves that dominate the jet dynamics at the resonant frequencies, the LES data at a given streamwise station is projected onto eigenmodes obtained from a locally parallel linear stability analysis that is described in the following section.

3.1. *Local Stability Analysis*

Stability analysis is performed around the LES turbulent mean flow. To obtain a smooth flow, the radial profile of the LES mean flow is fitted with the analytical profile

$$\overline{U}_x(r) = \frac{U_j}{2}\left[1 + tanh\left\{b\left(\frac{0.5}{r/D} - \frac{r/D}{0.5}\right)\right\}\right], \tag{3.1}$$

where b is the fitting parameter.

Fluctuating quantities are described by the vector $\mathbf{q}' = \begin{bmatrix} \boldsymbol{\rho}' & \mathbf{u}'_x & \mathbf{u}'_r & \mathbf{u}'_\theta & \mathbf{T}' \end{bmatrix}^\top$, where $\top$ represents the transpose, $\boldsymbol{\rho}'$ the density, $\mathbf{u}'_x$ the streamwise velocity, $\mathbf{u}'_r$ the radial velocity, $\mathbf{u}'_\theta$ the azimuthal velocity and $\mathbf{T}'$ the temperature. Normal-mode ansatz,

$$\mathbf{q}' = \hat{\mathbf{q}}(r)e^{i\alpha x}e^{im\theta}e^{-i\omega t}, \tag{3.2}$$

where $\hat{\mathbf{q}}$ gives the radial structure and α is the axial wavenumber, allows the linearised N-S equations to be compactly written as,

$$\mathbf{M}\hat{\mathbf{q}} = i\alpha\hat{\mathbf{q}}. \tag{3.3}$$

The eigenmodes are normalised such that each mode has: (1) 0^o phase angle for the streamwise velocity fluctuation at the jet axis ($\angle\hat{\mathbf{u}}_x = 0^o$ at $r = 0$); and (2) unit Energy norm, E (Chu 1965), defined as

$$\text{E} = \int_0^\infty \left[\frac{\overline{T}}{\gamma\overline{\rho}M_j^2} \mid \hat{\boldsymbol{\rho}} \mid^2 + \overline{\rho} \mid \hat{\mathbf{u}}_x \mid^2 + \overline{\rho} \mid \hat{\mathbf{u}}_r \mid^2 + \overline{\rho} \mid \hat{\mathbf{u}}_\theta \mid^2 + \frac{\overline{\rho}}{\gamma(\gamma-1)\overline{T}M_j^2} \mid \hat{\mathbf{T}} \mid^2\right] r\, dr. \tag{3.4}$$

Stability analysis is performed for $m = 0$ and over the frequency range, $0.23 \leqslant St \leqslant 0.47$. The eigenspectrum for one of the tonal frequencies, $St = 0.39$, is shown in figure 1(a).

Various families of modes can be seen in figure 1(a), where real and imaginary parts of α are represented on the horizontal and vertical axes respectively. The k_{KH}^+ (K-H mode marked with a square) is the only unstable mode of the system which leads to amplitude growth of the coherent part of the fluctuation field which then stabilises and decays, forming a wavepacket (Jordan & Colonius 2013).

The resonating modes leading to tones are marked with stars and are named as per Jordan *et al.* (2018). They are guided propagative modes resonating between the end locations and are the focus of the present work. The resonance loop consists of a downstream travelling mode (k_T^+) and an upstream travelling mode (k_d^- and/or k_p^-). Modes k_T^+ and k_d^- correspond to the acoustic waves trapped within the potential core and they belong to the families of the infinite number of such modes (marked by circles). Further details about these modes can be found in Towne *et al.* (2017), Schmidt *et al.* (2017) and Martini *et al.* (2019).

In figure 1(a), the modes in the first quadrant with subsonic phase speed (the sonic line is at $\alpha_r = \omega/c$) are stable and are distributed in two separate branches.: a near-horizontal branch consisting of critical layer modes that have support in the shear layer, and a near-vertical branch with eigenfunctions that have support in the core region of the jet (Rodríguez *et al.* 2015).

Although all guided modes are propagative at $St = 0.39$, this is not the case for all St. Figure 1(b) shows the trajectories of the four modes in the complex α plane as St varies from 0.23 to 0.47. At $St = 0.23$, k_T^+ and k_d^- are evanescent, and they move gradually towards the $\alpha_i = 0$ axis and overlap at saddle-point 1, defining a cut-on condition at $St = 0.37$ (Towne *et al.* 2017). The modes remain propagative until saddle-point 2, a cut-off condition, which occurs at 0.428, where k_T^+ and k_p^- modes meet. For $St > 0.428$, the k_T^+ and k_p^- modes become evanescent. At higher frequencies, other modes from the families of k_T^+ and k_d^- cut on leading to resonance, but these scenarios are not considered in the present work since the most energetic resonance occurs for the considered scenario.

3.2. *Educing mode amplitudes by bi-othogonal projections*

We here aim to educe amplitudes of the K-H mode, which is the main instability of the jet, and the three guided waves, which are postulated to be responsible for the observed tones. Due to the non-orthogonality of the system, mode amplitudes are obtained by bi-orthogonal projection as per Rodríguez *et al.* (2013, 2015).

A basis for bi-orthogonal projection is constructed from the adjoint system,

$$\mathbf{M}^H \hat{\mathbf{q}}^+ = i\alpha^+ \hat{\mathbf{q}}^+, \tag{3.5}$$

where H represents the Hermitian transpose, α^+ are the complex conjugate of eigenvalues of the direct system and $\hat{\mathbf{q}}^+$ are the adjoint eigenfunctions that we seek.

The adjoint eigenfunctions are normalized such that,

$$(\hat{\mathbf{q}}_i^+)^H \hat{\mathbf{q}}_i = 1, \tag{3.6}$$

where i is the index of the mode being normalized.

Before projection, $\hat{\mathbf{q}}_{LES}$ (from (2.1)) is interpolated onto the Chebyshev nodes, on which the eigenfunctions are defined, using Piecewise Cubic Hermite Interpolating Polynomials. Due to the fast decay of disturbances away from the jet, the points outside the available LES grid locations are assigned a value of 0 for the fluctuation quantities. This is corroborated by verifying that $\mid (\hat{\mathbf{q}}_i^+)^H \ \hat{\mathbf{q}}_i \mid$ is almost the same with or without this assumption $\forall St, \forall i$, and hence the projection amplitudes would be negligibly affected.

The mode amplitudes are then obtained by biorthogonal projection,

$$a_i^n = (\hat{\mathbf{q}}_i^+)^H \ \hat{\mathbf{q}}_{LES}^n, \tag{3.7}$$

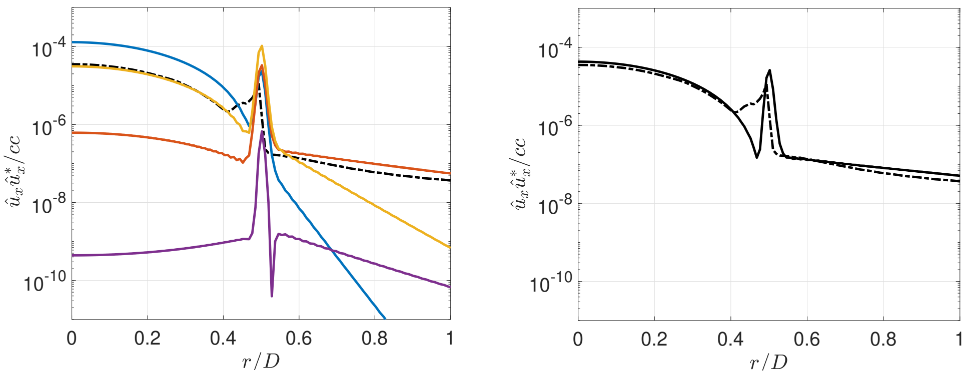

(a) Calibrated $\hat{\mathbf{u}}_x$ **(b)** Reconstructed $\hat{\mathbf{u}}_x$

Figure 2: Projections for $St = 0.39$, $m = 0$ at $x/D = 0$: (—, dashed black) LES; (—, blue) k_d^-; (—, red) k_p^-; (—, yellow) k_T^+; (—, purple) k_{KH}^+; (—, black) reconstruction from 4 modes.

where $\hat{\mathbf{q}}_{LES}^n$ is the LES fluctuation data from the n^{th} realisation; and a_i^n is the expansion coefficient that defines the contribution of the i^{th} mode to the flow state in the n^{th} realisation, giving the amplitude and the phase of mode.

In figure 2(a), radial profiles of the streamwise velocity for a selection of modes at the nozzle exit plane and for St = 0.39 are compared with the power spectral density (PSD) computed from the LES data. The guided modes have substantial magnitudes, consistent with the resonance phenomenon observed at this tonal frequency. It is also clear that within the jet core, the k_d^- and k_T^+ dominate the fluctuation field. In the shear region, k_d^-, k_p^- and k_T^+ have comparable levels. On the low-speed side of the shear layer, fluctuations are dominated by k_p^- and k_T^+. At the nozzle exit plane, negligible KH mode magnitude suggests a rank-3 system locally, but as the KH mode grows exponentially while travelling downstream, the system should be considered rank-4 globally.

A rank-4 reconstruction of the LES data, using these modes, is shown in figure 2(b) along with the LES fluctuation profile. At this resonance frequency, the rank-4 model provides a good overall description of the flow dynamics. We see that in the jet core, the reconstruction amplitude is lesser than the amplitude for the most dominant mode (see k_d^- in figure 2(a)). This is due to the destructive interference between the modes k_d^- and k_T^+ as we found them to be antiphase to each other. The mismatch for reconstruction in the mixing layer is likely due to disturbances originating in the nozzle boundary layer, leading to energetic but stable mixing layer modes (Towne & Colonius 2015).

4. Reflection-coefficient eduction

We now present a method used to compute reflection-coefficients between pairs of k^- and k^+ waves at the resonance end locations. Figure 3 shows a schematic of reflections at the nozzle exit plane and the turning point plane. At the turning point, the incident propagative k_T^+ wave can be reflected as a propagative wave (k_d^- or k_p^-) and transmitted as an evanescent wave. The reflected wave then propagates until it reaches the nozzle exit plane where it is reflected as a k_T^+ wave that travels downstream until the turning point, hence completing the resonance loop. The relation of magnitude and phases of these waves among each other are described by reflection and transmission coefficients at the corresponding end locations. Note that at the nozzle plane, apart from the contribution

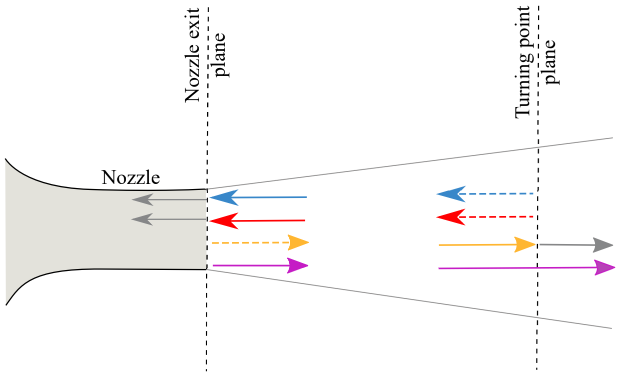

Figure 3: Sketch of waves interacting at the resonance end locations. At the nozzle exit plane: ($\longleftarrow$, blue) incident k_d^- wave; ($\longleftarrow$, red) incident k_p^- wave; ($\longleftarrow$, grey) transmitted waves; ($\longrightarrow$, dashed yellow) reflected k_T^+ wave; ($\longrightarrow$, purple) k_{KH}^+ wave. At the turning point plane: ($\longrightarrow$, yellow) incident k_T^+ wave; ($\longrightarrow$, grey) transmitted wave; ($\longleftarrow$, dashed blue) reflected k_d^- wave; ($\longleftarrow$, dashed red) reflected k_p^- wave.

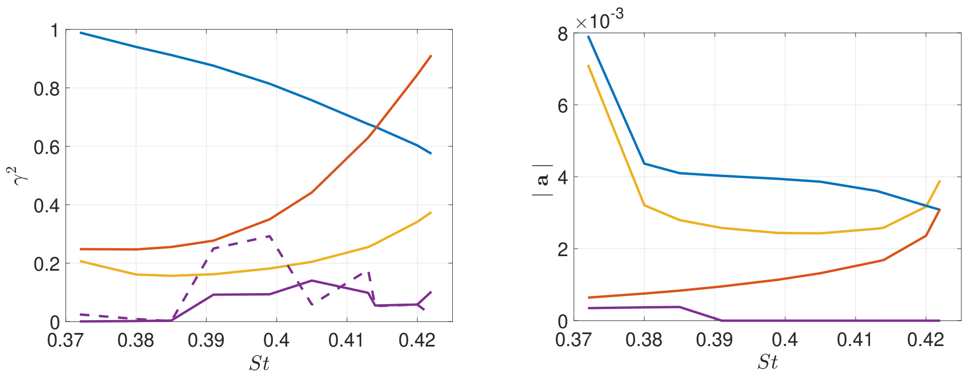

(a) Coherence function **(b)** Mode amplitudes

Figure 4: At the nozzle exit, $x/D = 0$. (a) Coherence function: (—, blue) k_d^-/k_T^+; (—, red) k_p^-/k_T^+; (—, yellow) k_d^-/k_p^-; (—, purple) k_d^-/k_{KH}^+; (—, dashed purple) k_p^-/k_{KH}^+. (b) Mode amplitudes: (—, blue) k_d^-; (—, red) k_p^-; (—, yellow) k_T^+; (—, purple) k_{KH}^+.

from k_d^- or k_p^- waves, k_T^+ wave may also be driven by nozzle fluctuations, or by the reflection of other k^- waves.

4.1. *Coherence analysis*

Before evaluating the reflection-coefficients, we examine the relation between expansion coefficient signals from the modes through the coherence function,

$$\gamma_{ij}^2 = \frac{\langle a_i a_j^H \rangle^2}{\langle a_i a_i^H \rangle \, \langle a_j a_j^H \rangle}, \tag{4.1}$$

where a_i and a_j are the expansion coefficients (see (3.7)) for the two modes, and $\langle \cdot \rangle$ represents the expected value, which is an estimate from the available samples.

For the present system of modes, coherence-function dependence on St at $x/D = 0$ can be seen in figure 4(a). For low St, a strong coherence is observed between k_d^- and k_T^+ which signifies that the k_d^-/k_T^+ resonance pair is active at these frequencies.

As St increases, the coherence function decays for k_d^-/k_T^+ while rising sharply for k_p^-/k_T^+. This suggests a change in the resonance mechanism, as frequency increases, towards a scenario where the k_p^-/k_T^+ pair is dominant. The small coherence of the k_{KH}^+ mode ($\gamma^2 < 0.3$) with the k^- waves signifies its absence in the resonance mechanisms, and for this reason, it is excluded from the forthcoming discussion.

The variation of mode amplitudes with St at $x/D = 0$, as shown in figure 4(b), tells a similar story. At low St, the k_T^+ amplitude decays with increasing St following the trend of k_d^-; but at high St, it grows with increasing St, following the trend of k_p^-, again reflecting a change of the dominant resonant mechanisms with increasing frequency.

4.2. *Reflection equations for nozzle exit plane*

At the nozzle exit plane, the expansion coefficients of the k_T^+ wave are related to expansion coefficients of k^- waves through complex reflection-coefficients as

$$a_T^+ = R^{d-}\ a_d^- + R^{p-}\ a_p^- + a_o. \tag{4.2}$$

Here, $R^{d-}\ a_d^-$ is the contribution to a_T^+ that arises from reflection of a_d^-; $R^{p-}\ a_p^-$ is the contribution from reflection of a_p^-; a_o groups all other contributions, e.g., reflections of other waves or disturbances coming from within the nozzle.

To evaluate the reflection-coefficients R^{d-} and R^{p-}, following the procedure of Bendat & Piersol (2011), we multiply (4.2) with both ${a_d^-}^H$ and ${a_p^-}^H$ and take the expected value, giving

$$\langle a_T^+ {a_d^-}^H \rangle = R^{d-} \langle a_d^- {a_d^-}^H \rangle + R^{p-} \langle a_p^- {a_d^-}^H \rangle + \langle a_o {a_d^-}^H \rangle, \tag{4.3}$$

$$\langle a_T^+ {a_p^-}^H \rangle = R^{d-} \langle a_d^- {a_p^-}^H \rangle + R^{p-} \langle a_p^- {a_p^-}^H \rangle + \langle a_o {a_p^-}^H \rangle. \tag{4.4}$$

Contributions from the nozzle boundary layer disturbances and other wave reflections are uncorrelated with the resonance dynamics, and thus we may assume $\langle a_o {a_d^-}^H \rangle = \langle a_o {a_p^-}^H \rangle = 0$. With this assumption, (4.3) and (4.4) can be solved, expressing the reflection-coefficients, R^{d-} and R^{p-}, in terms of expansion coefficient correlations.

4.3. *Reflection equations for turning point plane*

We now present the system of equations used to calculate the reflection-coefficients at the turning point location where the k_T^+ reflects as k_d^- and k_p^- (figure 3). Following a similar procedure to that of section 4.2, we can say that, at the turning point,

$$a_d^- = R_{d-}\ a_T^+ + a_o \qquad \& \qquad a_p^- = R_{p-}\ a_T^+ + a_o, \tag{4.5}$$

where R_{d-} and R_{p-} are the turning point reflection-coefficients.

Multiplying (4.5) with ${a_T^+}^H$ and taking the expected value gives,

$$\langle a_d^- {a_T^+}^H \rangle = R_{d-} \langle a_T^+ {a_T^+}^H \rangle + \langle a_o {a_T^+}^H \rangle \quad \& \quad \langle a_p^- {a_T^+}^H \rangle = R_{p-} \langle a_T^+ {a_T^+}^H \rangle + \langle a_o {a_T^+}^H \rangle. \tag{4.6}$$

With the assumption of $\langle a_o {a_T^+}^H \rangle = 0$, (4.6) can be solved for R_{d-} and R_{p-}.

5. Results and discussions

5.1. *Reflection-coefficients at the resonance end locations*

In the nozzle exit plane, the magnitudes and phases of the reflection-coefficients, R^{d-} and R^{p-}, are presented as a function of St in figures 5(a) and 5(b). High magnitudes for both the reflection-coefficients indicate strong reflections. We also observe that as St

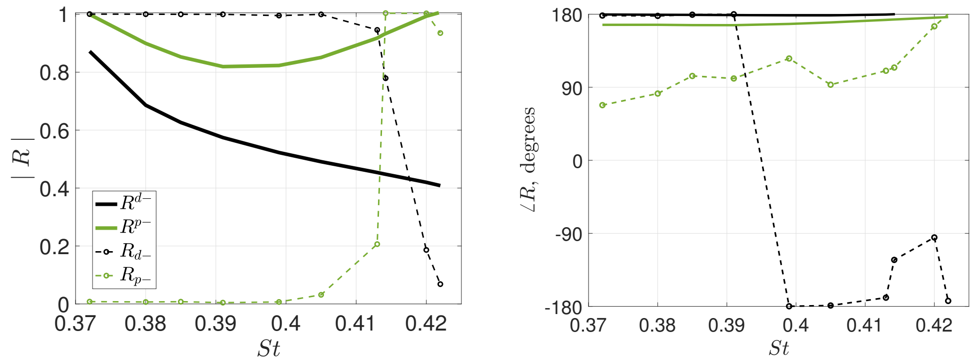

(a) Reflection-coefficient magnitude **(b)** Reflection-coefficient phase

Figure 5: Reflection-coefficients. At the nozzle exit: R^{d-} and R^{p-} correspond to the reflection of k_d^- wave and k_p^- wave respectively into the k_T^+ wave. At the turning point: R_{d-} and R_{p-} correspond to the reflection of k_T^+ wave into the k_d^- wave and k_p^- wave respectively.

increases, $\mid R^{d-} \mid$ decreases while $\mid R^{p-} \mid$ decreases and then increases. The phase angles for both reflection-coefficients are close to 180^o indicating out-of-phase reflection.

At the turning point, the magnitudes and phases of the reflection-coefficients are shown in figures 5(a) and 5(b) as well. From the local stability analysis, the k_T^+ mode is evanescent downstream of the turning point (see figure 1(b)). This implies perfect reflection in the turning-point plane, as beyond here, the k_T^+ mode cannot propagate energy downstream. This is exactly what is found for the reflection-coefficients in the turning-point plane i.e. $\mid R_{d-} \mid \sim 1$ & $\angle R_{d-} \sim 180^o$ for the lower St ($0.37 < St < 0.41$); and $\mid R_{p-} \mid \sim 1$ & $90 < \angle R_{p-} < 180^o$ for the higher St ($0.41 < St < 0.43$).

5.2. *Resonance-mechanism dependence on St*

The results from sections 4 and 5.1 conclude that for the frequency range $0.37 < St < 0.41$, it is the k_d^-/k_T^+ pair of modes that resonate while for $0.41 < St < 0.43$, it is the k_p^-/k_T^+ pair that resonate. The resonance mechanism switches near $St = 0.415$.

These two resonance mechanisms were proposed by Towne *et al.* (2017). For the lower frequencies, $St = 0.39$ for instance, the saddle point at the turning point exists between k_d^- and k_T^+ modes, which means that the acoustic resonance at $St = 0.39$ is being led by the k_T^+/k_d^- pair. This is exactly what we see in figures 4 and 5(a), where the k_d^-/k_T^+ pair of modes has strong coherence and large reflection-coefficient magnitudes.

For the reflections at the nozzle-exit plane at $St = 0.39$, the individual contributions of k_d^- and k_p^- to k_T^+ are better seen in figure 6(a) (see (4.2) for reference). The plot displays the square magnitude of mode amplitudes for k_T^+ (in yellow), as well as the contributions of k_d^- and k_p^- (in blue and red, respectively) across consecutive LES realizations. Figure 6(a) demonstrates that k_T^+ is primarily underpinned by reflection of k_d^-. Despite the high magnitude of R^{p-} at the nozzle-exit plane (figure 5(a)), the contribution of the k_p^- is much smaller than that of k_d^-, due its smaller amplitude (figure 4(b)).

For the higher frequencies, $St = 0.42$ for instance, the saddle point at the turning point exists between k_p^- and k_T^+ modes, hence the acoustic resonance is governed by the k_T^+/k_p^- pair. This is also what we observe in figures 4 and 5(a). The individual contributions of k_d^- and k_p^- to k_T^+ in the figure 6(b) shows that k_T^+ follows k_p^- much more closely than k_d^- at this St. Hence, k_T^+ is the direct reflection result of k_p^- at $St = 0.42$.

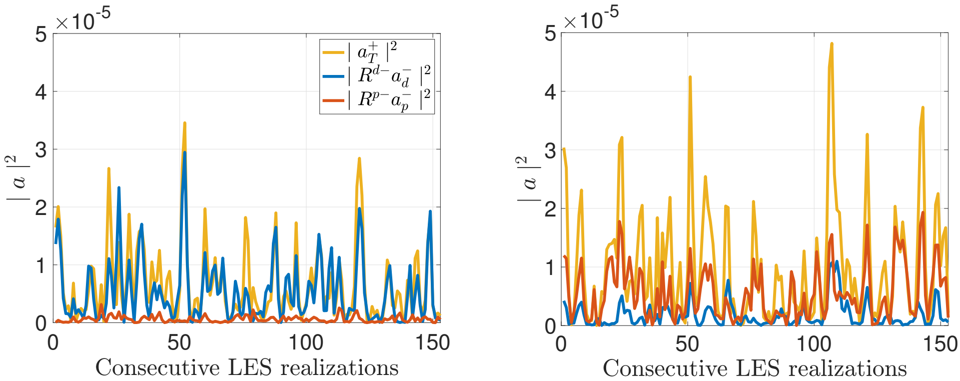

(a) For $St = 0.39$ **(b)** For $St = 0.42$

Figure 6: Contribution of k_d^- and k_p^- to k_T^+ at $x/D = 0$.

6. Conclusion

Resonating guided waves in the potential core of a $M = 0.9$ turbulent jet which lead to tones previously observed in experiments and numerical simulations (Towne *et al.* 2017; Brès *et al.* 2018) have been studied. The resonating guided waves consisted of a downstream-travelling duct-like wave (k_T^+), an upstream-travelling duct-like wave (k_d^-), and an upstream-travelling discrete free-stream wave (k_d^-).

Bi-orthogonal projection of LES data onto eigenmodes obtained from a linear stability analysis based on the turbulent was used to provide amplitudes of the resonating waves at the resonance end locations: the nozzle exit plane and downstream turning points. The dynamics of the flow at resonance frequencies are well described by a rank-4 model, comprising these neutrally stable guided waves and K-H instability waves. The reflection-coefficients at the resonance end locations were computed under the assumption that contributions from non-resonant modes are uncorrelated with the resonant modes. For the range of tonal frequencies, $0.37 < St < 0.43$, the mode amplitudes, coherence among them, and reflection-coefficients were presented.

Depending on the frequency, either of the k^- waves was found to be taking part in the resonance loop i.e. for $0.37 < St < 0.41$ (F1), the pair k_d^-/k_T^+ was active while for $0.41 < St < 0.43$ (F2), the pair k_p^-/k_T^+ was active. This frequency-dependence of resonance mechanism had exactly been postulated by Towne *et al.* (2017) where it was shown that the k_T^+ mode forms a turning point, the saddle point where upstream- and downstream-travelling waves exchange energy, with k_d^- mode in the F1 frequency range and with k_p^- mode in the F2 frequency range.

REFERENCES

Bendat, J. S. & Piersol, A. G. 2011 *Random data: analysis and measurement procedures*, , vol. 729. John Wiley & Sons.

Bers, A. 1983 Space-time evolution of plasma instabilities-absolute and convective. In *Basic plasma physics. 1*.

Bogey, Christophe 2021 Acoustic tones in the near-nozzle region of jets: characteristics and variations between mach numbers 0.5 and 2. *Journal of Fluid Mechanics* **921**.

Brès, G. A., Jordan, P., Jaunet, V., Le Rallic, M., Cavalieri, A. V. G., Towne, A., Lele, S. K., Colonius, T. & Schmidt, O. T. 2018 Importance of the nozzle-exit boundary-layer state in subsonic turbulent jets. *Journal of Fluid Mechanics* **851**, 83–124.

Briggs, R. J. 1964 Electron-stream interaction with plasmas .

Cavalieri, A. V. G., Jordan, P. & Lesshafft, L. 2019 Wave-packet models for jet dynamics and sound radiation. *Applied Mechanics Reviews* **71** (2).

Chu, Boa-Teh 1965 On the energy transfer to small disturbances in fluid flow (part i). *Acta Mechanica* **1** (3), 215–234.

Crighton, D. G. & Gaster, M. 1976 Stability of slowly diverging jet flow. *Journal of Fluid Mechanics* **77** (2), 397–413.

Edgington-Mitchell, Daniel 2019 Aeroacoustic resonance and self-excitation in screeching and impinging supersonic jets–a review. *International Journal of Aeroacoustics* **18** (2-3), 118–188.

Ho, Chih-Ming & Nosseir, Nagy S 1981 Dynamics of an impinging jet. part 1. the feedback phenomenon. *Journal of Fluid Mechanics* **105**, 119–142.

Huerre, Patrick & Monkewitz, Peter A. 1985 Absolute and convective instabilities in free shear layers. *Journal of Fluid Mechanics* **159** (-1), 151, citation Key Alias: huerre1985absolute.

Huerre, Patrick & Monkewitz, Peter A. 1990 Local and global instabilities in spatially developing flows. *Annual review of fluid mechanics* **22** (1), 473–537.

Jordan, P. & Colonius, T. 2013 Wave packets and turbulent jet noise. *Annual review of fluid mechanics* **45**, 173–195.

Jordan, P., Jaunet, V., Towne, A., Cavalieri, A. V. G., Colonius, T., Schmidt, O. & Agarwal, A. 2018 Jet–flap interaction tones. *Journal of Fluid Mechanics* **853**, 333–358.

Mancinelli, M., Jaunet, V., Jordan, P. & Towne, A. 2019 Screech-tone prediction using upstream-travelling jet modes. *Experiments in Fluids* **60** (1), 22.

Mancinelli, Matteo, Jaunet, Vincent, Jordan, Peter & Towne, Aaron 2021 A complex-valued resonance model for axisymmetric screech tones in supersonic jets. *Journal of Fluid Mechanics* **928**.

Martini, Eduardo, Cavalieri, André V. G. & Jordan, Peter 2019 Acoustic modes in jet and wake stability. *Journal of Fluid Mechanics* **867**, 804–834.

Michalke, A. 1970 A note on the spatial jet-instability of the compressible cylindrical vortex sheet .

Monkewitz, Peter A. & Sohn, Kihod 1988 Absolute instability in hot jets. *AIAA Journal* **26** (8), 911–916.

Powell, Alan 1953 On edge tones and associated phenomena. *Acta Acustica United with Acustica* **3** (4), 233–243.

Raman, Ganesh 1999 Supersonic jet screech: half-century from powell to the present. *Journal of Sound and Vibration* **225** (3), 543–571.

Rockwell, D & Naudascher, E 1979 Self-sustained oscillations of impinging free shear layers. *Annual Review of Fluid Mechanics* **11** (1), 67–94.

Rodríguez, D., Cavalieri, A. V. G., Colonius, T. & Jordan, P. 2015 A study of linear wavepacket models for subsonic turbulent jets using local eigenmode decomposition of piv data. *European Journal of Mechanics-B/Fluids* **49**, 308–321.

Rodríguez, D., Sinha, A., Brès, G. A. & Colonius, T. 2013 Inlet conditions for wave packet models in turbulent jets based on eigenmode decomposition of large eddy simulation data. *Physics of Fluids* **25** (10), 105107.

Rowley, Clarence W, Colonius, Tim & Basu, Amit J 2002 On self-sustained oscillations in two-dimensional compressible flow over rectangular cavities. *Journal of Fluid Mechanics* **455**, 315–346.

Schmidt, O. T., Towne, A., Colonius, T., Cavalieri, A. V. G., Jordan, P. & Brès, G. A. 2017 Wavepackets and trapped acoustic modes in a turbulent jet: coherent structure eduction and global stability. *Journal of Fluid Mechanics* **825**, 1153–1181.

Tam, Christopher KW & Ahuja, KK 1990 Theoretical model of discrete tone generation by impinging jets. *Journal of Fluid Mechanics* **214**, 67–87.

Towne, A., Cavalieri, A. V. G., Jordan, P., Colonius, T., Schmidt, O., Jaunet, V. & Brès, G. A. 2017 Acoustic resonance in the potential core of subsonic jets. *Journal of Fluid Mechanics* **825**, 1113–1152.

Towne, Aaron & Colonius, Tim 2015 One-way spatial integration of hyperbolic equations. *Journal of Computational Physics* **300**, 844–861.